inorganics

Article

Hydrogen Evolution Reaction, Electrochemical CO_2 Reduction, and Oxidative Photodegradation of Organic Dyes Catalyzed by Co(II) Trimethoxy-*Meso*-Arylporphyrin

Mouhieddinne Guergueb [1,*], Azhar Kechiche [1], Frédérique Loiseau [2], Florian Molton [2], Habib Nasri [1], Johannes Hohnsen [3] and Axel Klein [3,*]

[1] Laboratory of Physical Chemistry of Materials, Faculty of Sciences of Monastir, University of Monastir, Avenue de l'Environnement, 5019 Monastir, Tunisia
[2] Département de Chimie Moléculaire, Univ. Grenoble Alpes, CS 40700, CEDEX 9, 38058 Grenoble, France
[3] Faculty of Mathematics and Natural Sciences, Department of Chemistry, Institute for Inorganic Chemistry, University of Cologne, Greinstrasse 6, 50939 Cologne, Germany
* Correspondence: mouhieddinneguergueb@gmail.com (M.G.); axel.klein@uni-koeln.de (A.K.)

Abstract: In search of robust catalysts for redox transformations such as the hydrogen evolution reaction (HER) or CO_2 to CO reduction, we stepped on the previously reported *meso*-tetrakis(3,4,5-trimethoxyphenyl)porphyrinato cobalt(II) complex [Co(TTMPP)]. We prepared [Co(TTMPP)] in good yields and characterized it by IR, UV-vis absorption, photoluminescence spectroscopy, and cyclic voltammetry (CV). The [Co(TTMPP)] was used as a homogeneous catalyst for the electrochemical formation of H_2 (HER) in DMF (*N,N′*-dimethylformamide)/TFA (trifluoroacetic acid) and DMF/EtN_3BF_4 solutions, with high faradic efficiencies (*FE*). Additionally, the reduction of CO_2 to CO in DMF under a CO_2 atmosphere was catalyzed in DMF/TFE (TFE = 2,2,2-trifluoroethanol) and DMF/PhOH with high *FE* and only traces of H_2 as a by-product. Turnover frequencies of 15.80 or 9.33 s^{-1}, respectively were determined from CV experiments or controlled potential electrolysis in the presence of 1eq. TFE. They were lower with PhOH as proton source with 13.85 or 8.31 s^{-1}, respectively. Further, [Co(TTMPP)] as a solid catalyst (suspension) allowed the photodecomposition of the organic dyes methylene blue (MB) and rhodamine B (RhB) using H_2O_2 under visible light irradiation. The photocatalyst was photostable over five cycles. A photocatalytic mechanism was proposed based on trapping experiments of reactive oxygen species.

Keywords: Cobalt(II) porphyrin; cyclic voltammetry; electrocatalytic hydrogen evolution; electrocatalytic CO_2 reduction; photodegradation of dyes

check for updates

Citation: Guergueb, M.; Kechiche, A.; Loiseau, F.; Molton, F.; Nasri, H.; Hohnsen, J.; Klein, A. Hydrogen Evolution Reaction, Electrochemical CO_2 Reduction, and Oxidative Photodegradation of Organic Dyes Catalyzed by Co(II) Trimethoxy-*Meso*-Arylporphyrin. *Inorganics* **2023**, *11*, 6. https://doi.org/10.3390/inorganics11010006

Academic Editors: Duncan H. Gregory, Wolfgang Linert, Richard Dronskowski, Vladimir Arion, Claudio Pettinari and Torben R. Jensen

Received: 30 November 2022
Revised: 16 December 2022
Accepted: 17 December 2022
Published: 22 December 2022

1. Introduction

Cobalt porphyrin complexes combine the three oxidation states Co(I)/Co(II)/Co(III) with at least three of the intrinsic oxidation states of the porphyrin ligand $Por^{-}/Por^{2-}/Por^{3-}$ and thus show rich electrochemistry [1–9]. Consequently, they have been used for redox catalysis, [2,4,9–21] photocatalysis [9,11–13,17–21], and for related applications such as molecular sensing [8,21–23]. This last application owe Co(por) systems to the binding of additional ligands in the axial positions of the coordination plane defined by the tetradentate porphyrin ligand. This is less pronounced for the oxidation state Co(II) but very important to stabilize the oxidation state Co(III) [24], comparable to the biologically important B_{12} system (a Co corrin) [25]. Amongst the Co porphyrins, the *meso*-tetraphenyl porphyrin complexes with *meso*-tetrakis(phenyl)-porphyrin cobalt(II) [Co(TPP)] (Scheme 1a) as the parent compound, have turned out to be the most interesting group, since the phenyl groups allow vast substitution to vary the redox potentials [1–10,26–28], to confine the metal center through bulky substituents, to introduce charged moieties such as the SO_3^{-} group, and to modify their solubility in water or organic solvents [2–4,9–14,27,29,30]. Amongst important electrocatalytic processes catalyzed by [Co(TPP)] derivatives, the hydrogen evolution reaction (HER) which is the catalytic reduction of protons [2,9,10,31–41], the reduction or evolution of O_2 [2,32,39,40,42–45], and the CO_2 to CO reduction [2,9,15,16,46–59] have gained enormous importance in view of the growing need to produce the environmental benign fuels H_2 and O_2 for fuel cell applications and energy conversion and to use waste CO_2 for the production of CO as a versatile C1 building block for base chemicals. Another important application of [Co(TPP)] and derivatives as catalysts is the oxidative degradation of organic pollutants [9–13,17–19,60].

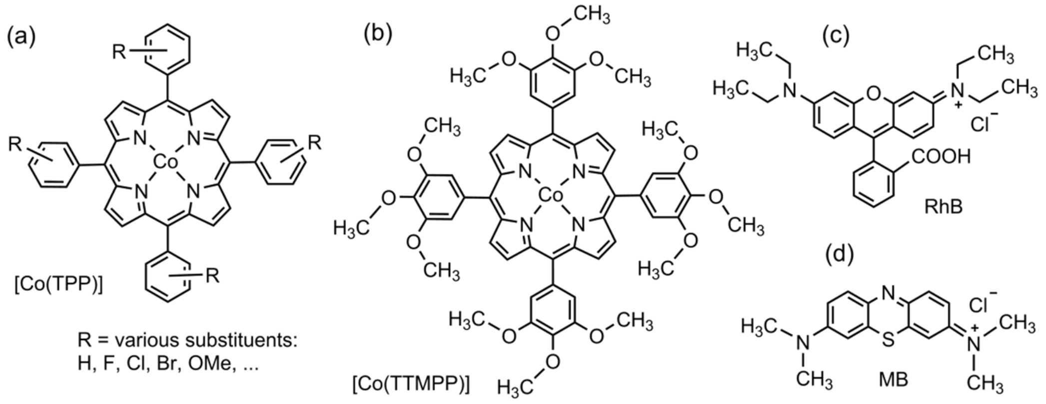

Scheme 1. Structures of the prototypical [Co(TPP)] (R = H) with phenyl-substituted derivatives [Co(TPP-R_4)] (**a**), [Co(TTMPP)] (**b**), rhodamine B (RhB) (**c**), and methylene blue (MB) (**d**).

We and others have contributed to this field by studying [Co(TPP)] catalysts containing various substitution patterns at the *meso*-phenyl groups (Scheme 1a) in catalytic [2,14,26,61–64] and electrocatalytic reactions [2,4,9,10,21,49,52,56] and in oxidative degradation reactions of organic dyes [9–13,18,19].

Herein, we report the preparation of the previously reported [64–67] *meso*-tetrakis(3,4,5-trimethoxyphenyl)porphyrinato cobalt(II) complex [Co(TTMPP)] (Scheme 1b), its characterization through elemental analyses, ESI-MS(+) and FT-IR, UV-vis absorption, and fluorescence spectroscopy alongside with its electrochemical behavior. We also report the use of [Co(TTMPP)] as a catalyst in the electrocatalytic evolution of H_2 (HER), for the electrocatalytic reduction of CO_2 to CO, and for the photo-assisted oxidative degradation using H_2O_2 of the dyes methylene blue (MB) and rhodamine B (RhB) (Scheme 1c,d).

2. Results and Discussion

2.1. Synthesis and Analysis

The free base porphyrin H_2TTMPP was prepared and purified, adopting a reported procedure [68] with an isolated yield of 70%. Elemental analysis (see Experimental Section) and FT-IR spectroscopy (Figure S1, Supplementary Materials) showed its purity. The Co(II) complex [Co(TTMPP)] was synthesized in 93% yield using the dimethylformamide procedure [9] and analyzed by elemental analysis,^{1}H NMR (Figure S2), ESI-MS(+) (Figure S3), and FT-IR spectroscopy (Figure S1), for details, see Experimental Section. The ^{1}H NMR spectrum showed broad signals due to the paramagnetic character of the Co(II) complex [64].

2.2. Photophysical Properties

The UV-vis absorption spectrum of H_2TTMPP is characterized by an intense absorption band at 424 nm known as the Soret band and four less intense absorption bands at 520, 556, 598, and 652 nm known as the Q bands(Figure 1a) [9,12]. For [Co(TTMPP)], the Soret band is found at 414 nm, thus blue-shifted compared to H_2TTMPP alongside with two Q bands at 532 and 567 nm, compared to the four observed for the free base. These changes are due to the increase in symmetry from C_{2v} to D_{4h} upon coordination [9,12,13,18,69]. The optical band gap (*E*g-op) was calculated using the 1240/λ_{gap} method to 1.84 eV (λ_{gap} = 674 nm) for H_2TTMPP and 2.08 eV (λ_{gap} = 596 nm) for [Co(TTMPP)]. The value found for [Co(TTMPP)] is typical for Co(II) porphyrins [8,9,11–13].

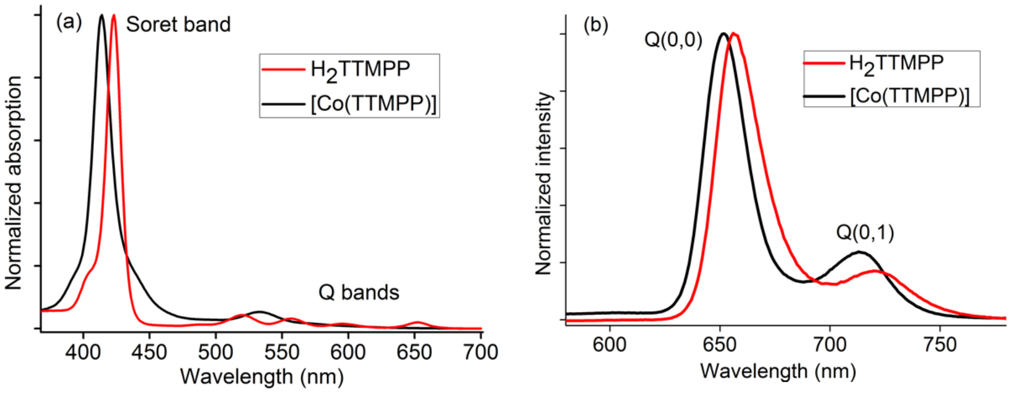

Figure 1. Normalized UV-vis absorption spectra (**a**) and photoluminescence spectra (λ_{exc} = 430 nm) (**b**) of [Co(TTMPP)] and H_2TTMPP in CH_2Cl_2.

Upon excitation at 430 nm, both H_2TTMPP (λ_{max} = 658 and 721 nm) and [Co(TTMPP)] (λ_{max} = 651 and 714 nm) show photoluminescence (PL) in CH_2Cl_2 at room temperature (Figure 1b). They can be assigned to the S_1[Q(0,0)] → S_0 and S_1[Q(0,1)] → S_0 transitions in agreement with previous studies on [Co(TPP)] and derivatives [9,12,13,18]. The PL quantum yields (Φ_{PL}) are 0.082 for H_2TTMPP and 0.027 for [Co(TTMPP)] with lifetimes of 7.1 ns for H_2TTMPP and 1.3 ns for [Co(TTMPP)] which are in the typical range for *meso*-arylporphyrins and their Co(II) complexes [3,9,12,13,18].

2.3. Electrochemical Characterization of [Co(TTMPP)]

Cyclic voltammetry on [Co(TTMPP)] was performed in *N*,*N*-dimethylformamide (DMF) at room temperature, showing two reversible reduction waves and two reversible oxidation waves (Figure 2). The first reversible one-electron oxidation at 0.26 V vs. SCE is attributed to the Co(II)/Co(III) redox couple in line with previous reports [5,7,9]. From other [Co(TPP)] derivatives and further M(II) porphyrins it is also known that after oxidation solvents coordinate to Co(III), here DMF, thus influencing the potential [9,28,62,70].

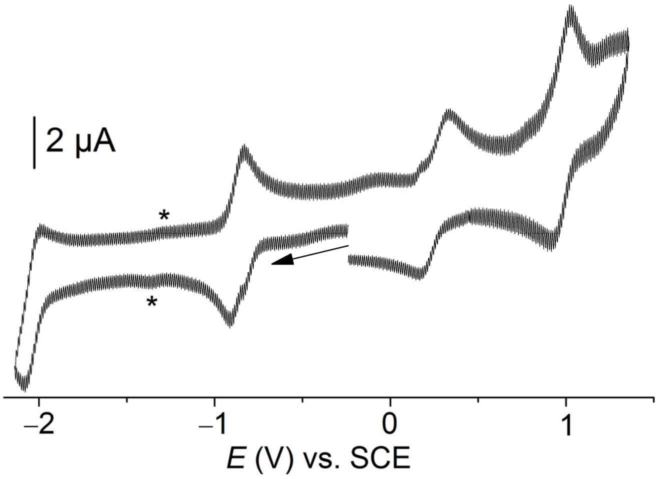

Figure 2. Cyclic voltammogram of [Co(TTMPP)] in 0.1 M *n*-Bu_4NBF_4/DMF under Ar at a scan rate of 100 mV s^{-1}. The * mark a wave which might be due to traces of O_2.

A second, slightly larger oxidation wave was observed at 0.97 V and is assigned to a porphyrin-centered process ($\text{Por}^{2--}/\text{Por}^{1-}$), in agreement with previous reports [5,7,9]. The first reduction $E_{1/2} = -0.86$ V is attributed to the Co(II)/Co(I) redox couple [5,9,28], the second at $E_{1/2} = -2.04$ V to a $\text{Por}^{2-}/\text{Por}^{3-}$ redox couple in line with previous reports [9,28]. The values for [Co(TTMPP)] are very similar to those of the recently studied 4-CF_3 derivative *meso*-tetrakis(4-(trifluoromethyl)phenyl)porphyrinato Co(II) [Co(TMFPP)] (−2.05, −0.91, 0.30, and 0.98 V) [9] in line with a small to the marginal influence of the substituents on the *meso*-phenyl rings found also in other studies [3–5,9,27,28,70].

Applying scan rates from 250 to 1000 mV/s (Figure 3a) allowed us to calculate the diffusion coefficient (D) of the complex from the Randles–Sevcik equation (Equation (1)) which applies for fully homogeneous diffusion-controlled electrochemical process saying that the peak current (I_p) for a faradaic electron transfer varies linearly with the square root of the scan rate ($\nu^{1/2}$). D can be calculated from the slope of I_p vs. $\nu^{1/2}$ (Figure 3b).

$$I_p = 0.4463\, F\, A\, (F/RT)^{1/2}\, D^{1/2}\, {n_p}^{3/2}\, [C_0]\, \upsilon^{1/2} \tag{1}$$

where I_p is the peak current, F is the Faraday constant (96,485 C mol^{-1}), R is the universal gas constant (R = 8.314 J K^{-1} mol^{-1}), T = 298 K, n_p is the number of electrons transferred (here, $n_p = 1$), and A is the active surface area of the electrode (0.00785 cm^2). Note that our plots are reported as a function of the current density, bypassing the need of the area value in equation 1. Here, $[C_0]$ is the concentration of the analyte (here $[C_0]$ = 1 mM), and ν is the scan rate in V s^{-1}.

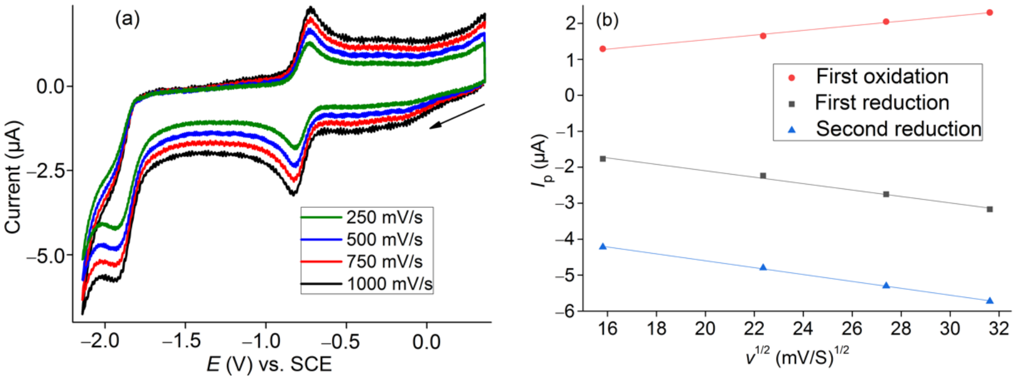

Figure 3. (**a**) Cyclic voltammograms of [Co(TTMPP)] in 0.1 M $n\text{-}Bu_4NBF_4$/DMF under an Ar atmosphere recorded at different scan rates. (**b**) Peak currents vs. square roots of the scan rate for the two reductions and the first oxidation process.

D for the Co(II)/Co(I) reduction was determined to 1.8 10^{-7} cm S^{-1}, which is larger than the 2.3 10^{-8} cm S^{-1} determined for the porphyrin reduction ($\text{Por}^{2-/}\text{Por}^{3-}$). The difference is attributable to the growth of the negative charge. These results are very similar to those obtained previously with the [Co(TMFPP)] complex (1.98 10^{-7} cm S^{-1} and 1.1 10^{-8} cm S^{-1}, respectively) [9]. D for the first oxidation was determined to 7.2 × 10^{-7} cm S^{-1}. The pretty large value is in keeping with the assumed additional DMF ligand for the oxidized complex $[\text{Co(TTMPP)(DMF)}]^+$.

2.4. Electrocatalytic H_2 Production

In a recent study, the electrocatalyzed H_2 evolution using the Co(II) complex $[\text{Co(bapbpy)Cl}]^+$ (bapbpy = 6,6′-bis(2-aminopyridyl)-2,2′-bipyridine) was carried out in DMF and different mechanisms were described depending on the strength of the acid used as proton source [71]. We thus studied the electrocatalytic activity of [Co(TTMPP)] as homogeneous catalyst for H_2 production in DMF using trifluoroacetic acid (TFA) and triethylammonium tetrafluoroborate ($HNEt_3BF_4$) as proton sources. Upon addition of TFA or $HNEt_3BF_4$ in DMF, the CVs of [Co(TTMPP)] show catalytic reduction waves at around −2 V which coincide with the second reduction wave of [Co(TTMPP)], whereas the first reduction wave at around −0.9 V remains unchanged (Figure 4 and Figure S4, Supplementary Material). As for the previously reported TPP-CF_3 complex [Co(TMFPP)] [9], the first reduced species $[Co(I)(Por^{2-})]^-$ is not catalytically active for [Co(TTMPP)] and efficient proton reduction required the double reduced species which can be described as either $[Co(0)(Por^{2-})]^{2-}$ or $[Co(I)(Por^{3-})]^{2-}$. The catalyst [Co(TCPP)] (H_2TCPP = *meso*-tetra-*para*-X-phenylporphine) showed a behavior similar to [Co(TTMPP)] for X = Cl, whereas the X = OMe or H derivatives reduced protons catalytically already at around −1 V [10]. Maybe the character of the second reduction is very sensitive to the substitution pattern. Alternatively, the reactive two-electron reduced species might be generated through a disproportionation reaction: 2 $[Co(Por)]^-$ = [Co(Por)] + $[Co(Por)]^{2-}$ for the complexes with X = OMe or H and this reaction is again depending on the substitution pattern. This remains to be studied in more detail and will be further discussed in Section 2.5.

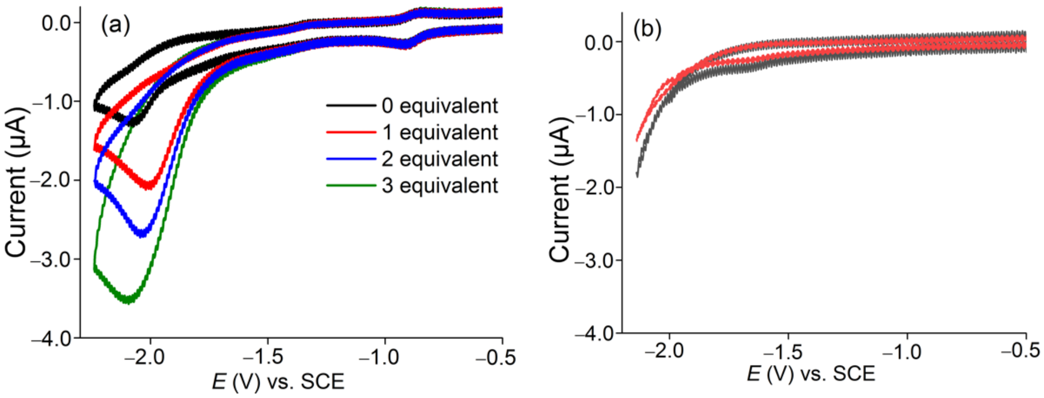

Figure 4. (**a**) CVs of [Co(TTMPP)] (1 mM) in the absence (black trace) or in the presence of 1 to 3 equivalents $HNEt_3BF_4$ in DMF at 250 mV s^{-1}. (**b**) Blank experiments with no or 1 equivalent of $HNEt_3BF_4$ without catalyst.

Controlled potential electrolysis (CPE) at −2 V for 2 h in aqueous DMF under an Ar atmosphere gave a faradaic efficiency (FE) of 76% in the presence of three equivalents TFA (Table 1). Gas chromatography (GC) confirmed the production of H_2 (Figure S5) during CPE. The catalytic current enhancement (I_{cat}/I_p) where I_{cat} is the catalytic current after the addition of a proton source and I_p is the peak current in the absence of acid is 10.86, the turnover number (TON) is 11.04, and the turnover frequency (TOF) 5.52 h^{-1}. In the presence of three equivalents $HNEt_3BF_4$, CPE at −1.89 V for 2 h in DMF under an argon atmosphere we recorded a higher FE of 88%. In addition, I_{cat}/I_p (13.65), the TON (14.6), and TOF (7.3 h^{-1}) values are superior for $HNEt_3BF_4$ over TFA.

Table 1. Important parameters for the electrocatalytic H_2 evolution [a].

H^+ Source	**Time $_{CPE}$**	**E_{CPE}**	**I_{cat}/I_p**	**FE_{H2}**	**TON**	**TOF (h^{-1})**
3 eq. TFA	2 h	−2.00	10.86	76	11.04	5.52
3 eq. $HNEt_3^+$	2 h	−1.89	13.65	88	14.60	7.30

[a] Under CPE conditions using [Co(TTMPP)] as catalyst in 0.1 M *n*-Bu_4NBF_4/DMF under an Ar atmosphere. E_{CPE} = applied potential, FE = faradaic efficiency, TON = turnover number, TOF = turnover frequency.

The FE for [Co(TTMPP)] in the presence of $HNEt_3BF_4$ is also slightly higher than the one found for the [Co(TMFPP)] complex (85% using DMF/acetic acid) [9] and overall these values are comparable to those of other Co(II) porphyrin derivatives with various *meso*-substituents [10,31,32,36,40,41,71]. For example, the complexes $[Co(TMAP)](ClO_4)_2$ (H_2TMAP = *meso*-tetrakis(*N*,*N*,*N*-trimethylanilinium-4-yl)porphine), $[Co(TMPyP)](ClO_4)_2$ (*meso*-tetrakis(*N*-methylpyridinium-4-yl)porphine), and [Co(TpyP)] (*meso*-tetrakis-4-ylporphine) showed FEs around 90% when using TFA as proton source [41]. For [Co(TMAP)] (H_2TMAP = *meso*-

tetrakis(*N*,*N*,*N*-trimethylanilinium-4-yl)porphine) an FE of almost 68% was reported when using acetic acid as proton source [10]. Our experiments revealed a high sensitivity to the efficiency of the proton source and it is clear that direct comparison with results of studies using different proton sources is difficult.

Markedly higher TONs of 28 and 35 have been recently reported for the above-mentioned polypyridyl Co(II) complex $[Co(bapbpy)Cl]^+$ [71] at overpotentials of >0.8 V, whereas at an overpotential of <0.6 the TON drops to 4 (with HBF_4 as proton source).

2.5. Electroreduction of CO_2 to CO

2.5.1. Catalytic Behavior under CO_2

The electrocatalytic behavior of [Co(TTMPP)] as a homogeneous catalyst in CO_2 reduction was studied in CO_2-saturated DMF solutions with trifluoroethanol (TFE) or phenol (PhOH) as H^+ sources. Cyclic voltammograms in the presence of CO_2 show catalytic currents at around −2 V (Figure 5 and Figure S6). Upon the addition of protons without CO_2, similar catalytic currents were observed. Slightly higher currents were found for the combination of CO_2 and protons with I_{cat}/I_p values of 5.6 for TFE and 4.9 for PhOH. As observed for the proton reduction, the first reduced species $[Co(I)(Por^{2-})]^-$ seems not to be catalytically active for the CO_2 reduction, whereas the double reduced species ($[Co(0)(Por^{2-})]^{2-}$ or $[Co(I)(Por^{3-})]^{2-}$) appears to be active. The same was previously found for the TPP-CF_3 derivative [Co(TMFPP)] [9].

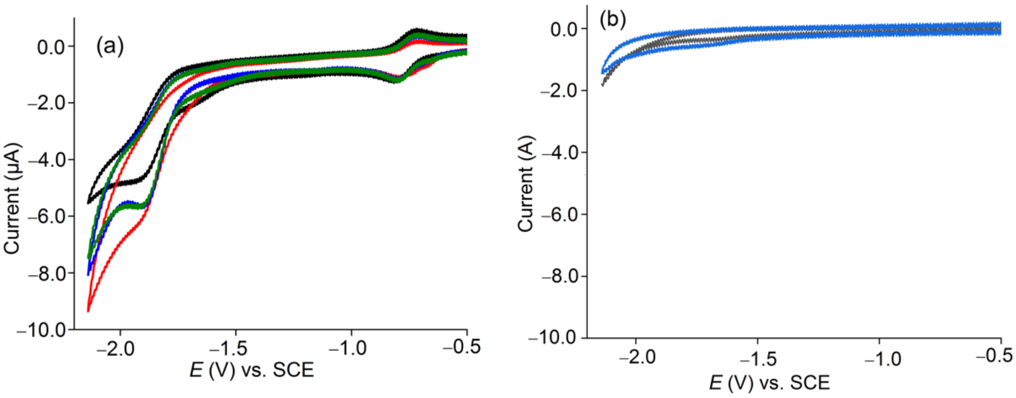

Figure 5. (**a**) Cyclic voltammograms of 1 mM solutions of [Co(TTMPP)] in 0.1 M n-Bu_4NBF_4/DMF in the absence of PhOH (black: in Ar, green: in CO_2) and in the presence of 1 mM of PhOH (blue: in Ar, red: in CO_2). (**b**) Blank test in the absence (black) or presence (blue) of PhOH, without catalyst.

The catalytic performance was studied under CPE conditions at −1.94 V and −1.93 V in DMF under a CO_2 atmosphere in the presence of PhOH (Figure 5) or TFE (Figure S6) and faradaic efficiencies (FEs) of 95% and 88% were found (Table 2). GC confirmed the production of CO and no detectable amounts of H_2 (Figure S7). From this, we conclude that in the presence of CO_2, the protons only cause a lowering of the overpotential of the CO_2 to CO reduction but are not reduced [9,15,47,50–54,57,58]. For the CF_3-substituted derivative [Co(TMFPP)], we recently obtained an FE of 90% in aqueous DMF [9], whereas for the standard [Co(TPP)] only 50% were found under similar conditions [15]. Remarkably, when immobilized on carbon nanotubes, [Co(TPP)] gave efficiencies of 83% or 93% at −1.15 and −1.35 V, respectively [15]. We can thus conclude that both CF_3 and OMe substitution enhanced the efficiency for the CO_2 reduction using [Co(TPP)] derivatives, whereas the applied potentials are in the same range as for [Co(TPP)]. Support with an electron-conducting material could pave the way for the use of [Co(TTMPP)] as an electrocatalyst at less negative potentials [15,16,30,42,46,51,54,72].

Table 2. Faradaic efficiencies of the CO_2 reduction [a].

H^+ Source	Time $_{CPE}$	E_{CPE}	FE_{CO2}	FE_{H2}
1 eq. TFE	2 h	−1.94	95	Not detected
1 eq. PhOH	2 h	−1.93	88	

[a] Under CPE conditions using [Co(TTMPP)] as catalyst in 0.1 M *n*-Bu_4NBF_4/DMF under a CO_2 atmosphere. E_{CPE} = applied potential, FE = faradaic efficiency.

Mechanistic studies suggest CO_2 activation by the singly reduced species $[Co(I)(Por^{2-})]^-$ with subsequent protonation to $[Co(II)(COOH)(Por^{2-})]$. Further protonation and H_2O loss lead to $[Co(III)(CO)(Por^{2-})]$ [2,58] and one-electron reduction back to the parent Co(II) complex [2]. As a side reaction, $[Co(I)(Por^{2-})]^-$ reacts with H^+ forming a hydrido complex $[Co(III)(H)(Por^{2-})]$ which reacts with H^+ to yield H_2 [2]. As pointed out above, we did not observe H_2 production. The proton source just facilitated the CO_2 to CO conversion and from our experiments, we conclude that the potentials of the two one-electron reduction steps for the CO_2 reduction might be markedly different depending on the porphyrin substitution pattern and the proton source [58]. This remains to be studied in more detail.

2.5.2. Benchmarking of the Catalyst

The efficiency of an electrocatalyst is a function of its overpotential, the inherent turnover frequency (TOF, cycles completed per second), the number of turnovers (TON, the maximum number of cycles for one mol of catalyst), and the speed of catalysis expressed as the maximum TOF (TOF_{max}) [73,74]. The ratio I_{cat}/I_p measured at different scan rates gives a good estimation of the TOF_{max}. The catalytic plateau current (I_{cat}) can be expressed as in Equation (2) assuming the electron transfer to the catalyst is fast and the typical S-shaped feature of the current is observed [73,74].

$$I_{cat} = n_{cat}\ F\ A\ [C_0]\ (D\ k_{cat}\ [CO_2])^{1/2} \tag{2}$$

The catalysis follows the first-order rate in both the catalyst and substrate. Combining Equations (1) and (2), the maximum turnover frequency $TOF_{max} = k_{cat}\ [CO_2]$ can be determined using Equation (3) from the cyclic voltammograms recorded in CO_2-saturated DMF solution in presence of TFE or PhOH.

$$TOF_{max} = k_{cat}\ [CO_2] = (F\ v\ np^3/R\ T)(0.4463/n_{cat})^2(I_{cat}/I_p)^2 \tag{3}$$

For both Equations (2) and (3), n_{cat} is the number of electrons required for the catalytic reaction (n_{cat} = 2), n_p = number of transferred electrons (here = 1), ν is the scan rate, F is the Faraday constant (96,485 C mol^{-1}), A is the surface area of the electrode (A = 0.00785 cm^2), C_{cat} is the catalyst concentration ($[C_0] = 10^{-3}$ M), D_{cat} is the diffusion constant of the catalytically active species, k_{cat} is the rate constant of the catalytic reaction, and $[CO_2]$ is the concentration of CO_2 in DMF (Figures S8 and S9).

The thus determined TOF_{max} values for [Co(TTMPP)] are 15.80 s^{-1} and 13.85 s^{-1} for 1 equivalent TFE and 1 equivalent PhOH, respectively. TOFs for Co-based catalysts were reported to range from 0.2 to >1000 s^{-1} [47] and for supported [Co(TPP)] values of 2.5 to 8.7 s^{-1} were reported depending on the C-support [48,50]. Thus, [Co(TTMPP)] showed good performance in solution even without support. At the same time, it is difficult to compare homogeneous and heterogeneous catalysts and most [Co(TPP)] electrocatalysts were used as supported [47–51] or encapsulated [45,46] heterogeneous catalysts.

Catalytic Tafel plots allow examining the catalytic performances against both kinetic (TOF_{max}) and thermodynamic (overpotential, η) descriptors [2,73,74]. In DMF, the standard potential of the CO_2/CO couple can be described through Equation (4) [73,74]:

$$E^0{}_{CO2/CO,DMF,HA} = -0.259 - 0.0529\ \text{pka(HA,DMF)} \tag{4}$$

with $pka^{TFE} = 24.0$ and $pka^{PhOH} = 18.8$ in DMF [7] and overpotential can be determined as shown in Equation (5):

$$\eta = |E^0_{CO2/CO} - E_{app}| \tag{5}$$

The TOF was plotted against the overpotential (Figure 6) applying Equation (6):

$$TOF = TOF_{max}/(1 + \exp(F/(R\,T)(E^0_{CO2} - E_{cat}))\exp(-(F\,\eta)/(R\,T)) \tag{6}$$

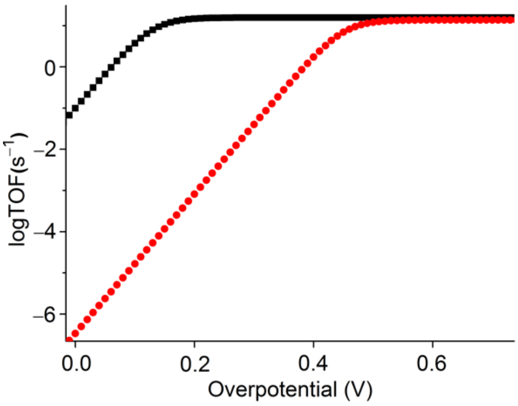

Figure 6. Catalytic Tafel plots of [Co(TTMPP)] with 1 eq. TFE (black) and with 1 eq. PhOH (red).

In this electroanalytical method, competing factors such as substrate depletion and catalyst inhibition are minimized by analyzing the foot of the catalytic wave to determine the observed catalytic rate constant (k_{cat}) [74]. From plots of I/Ip versus $1/\{1 + \exp[(F/RT)(E - E_{cat/2})]\}$, k_{cat} can be calculated from the slope of the linear portion of the curve, which gives access to the maximum TOF value, where TOF = $k_{cat}[CO_2]$ under saturation conditions [2,73–75]. Under CPE conditions, scan-rate-independent TOFs of 9.33 and 8.31 s^{-1} were determined, whereas the same method gave slightly larger values (15.80 and 13.85 s^{-1}) from CVs (Table 3). These values are comparable to those found for other Co porphyrin derivatives with various *meso*-substituents [2,15,16,46–51,54,56,72]. UV-vis absorption spectra of the solution before and after the CPE experiments show that the [Co(TTMPP)] complex is almost quantitatively retained after 2 h of CPE, indicating good stability of the catalyst (Figure S10).

Table 3. Catalytic parameter for the CO_2/CO reduction [a].

H^+ Source	**E_{CPE}**	**I_{cat}/I_p**	**TOF(s^{-1})**		**TON [b]**
			CPE	**CVs**	
1eq. TFE	−2	5.6	9.33	15.80	113,760
1eq. PhOH	−2	4.9	8.31	13.85	99,720

[a] From the Tafel plots (Figure 6). [b] From the CVs Figures S8 and S9.

2.6. Photocatalytic Degradation of Methylene Blue and Rhodamine B Using H_2O_2

UV-vis absorption spectroscopy allowed following the oxidative photodegradation of the two dyes methylene blue (MB) and the rhodamine B (RhB) in H_2O using H_2O_2 as oxidant and [Co(TTMPP)] as solid heterogeneous catalyst Figures 7 and S11).

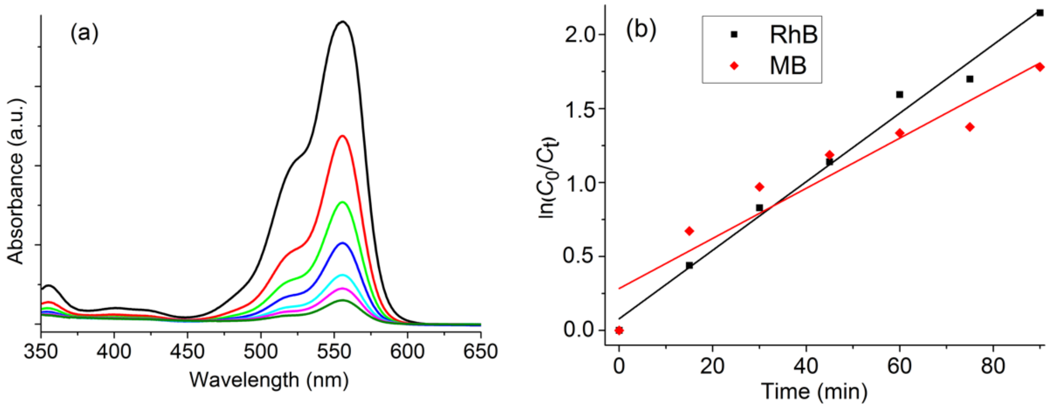

Figure 7. (**a**): Evolution of the absorbance of RhB over time (black (start), red (15 min after H_2O_2 addition), green (30 min), blue (45 min), cyan (60 min), pink (75 min), olive (90 min) in H_2O at pH = 7 and 25 °C; 0.024 mmol of [Co(TTMPP)], C_{dye} = 0.05 mmol, C_{H2O2} = 0.06 mmol. (**b**): Changes in $\ln(C_t/C_0)$ over time for both dyes.

The degradation efficiencies after 90 min under visible light irradiation were determined to be 92.6% for RhB and 84.1% for MB. In the absence of light, degradation was lower than 1%. These values are similar to those recently reported for the [Co(TMFPP)] derivative [9], and markedly higher compared to those of [Co(TMPP)(4-CNpy)] and [Co(TClPP)(4-CNpy)] which were up to 80% for MB after 300 min reaction time [18]. Comparison of R^2 showed that the reactions follow pseudo-first-order kinetics with $\ln(C_0/C_t) = k\,t$, where C_0 is the initial dye concentration, C_t is the dye concentration at time t, and k is the rate constant. The rate constants k were calculated to 0.023 for RhB and 0.017 min^{-1} for MB (Figure 7b).

Recycling experiments with five cycles showed only a slight reduction of activity (Figure S12) with efficiencies decreasing from 91.2% to 88.2% for PhB and from 84.1% to 80.3% for MB after five cycles (90 min each). Importantly, parts of the loss of catalytic activity are caused by the unavoidable loss of photocatalyst during recovery.

To get more insight into the photodegradation mechanism of RhB and MB using our catalyst, the influence of potentially active species such as superoxide radicals ($^{\bullet}O_2^{-}$), hydroxyl radicals ($^{\bullet}OH$), or holes (h^+) in the reaction [17,60] was investigated using several types of scavengers: *L*-ascorbic acid for ($^{\bullet}O_2^{-}$), isopropyl alcohol (IPA) for ($^{\bullet}OH$), and sodium ethylene diamine tetraacetate $Na_2(H_2EDTA)$ for hole trapping [76]. The addition of IPA led to a marked decrease in the degradation efficiency to 50.1% for RhB and 44.3% for MB. The addition of *L*-ascorbic acid reduces the rates even to 28.3% for RhB and 21.3% for MB. In contrast to this, the addition of $Na_2(H_2EDTA)$ reduced the efficiency only to 90.2% for RhB and 81.5% for MB. We therefore conclude that holes play only a minor role in the photodegradation of RhB and MB, whereas ($^{\bullet}OH$) and ($^{\bullet}O_2^{-}$) are the predominant species.

3. Experimental Section

3.1. Materials

N,*N*-Dimethylformamide (DMF, >99.8%, extra dry over molecular sieves), *N*,*N*-diisopropylethylamine (DIPEA), $Co(OAc)_2{\cdot}4H_2O$, *p*-chloranil, NEt_3, CH_2Cl_2, $CHCl_3$, *n*-hexane, EtOH, trifluoroacetic acid (TFA), and BF_3 OEt_2 (all Acros Organics); $HNEt_3BF_4$, rhodamine B (RhB), methylene blue (MB), H_2O_2, 3,4,5-trimethoxybenzaldehyde, pyrrole, H_2O_2 (30%), ethyl acetate (AcOEt), isopropyl alcohol (IPA), *L*-ascorbic acid, sodium ethylene diamine tetraacetate $Na_2(H_2EDTA)$ (all Sigma-Aldrich, Merck, Darmstadt, Germany); CF_3CH_2OH (TFE) and phenol (PhOH) (both Alfa-Aesar, Thermo Fisher, Kandel, Germany); *n*-Bu_4NBF_4 and *n*-Bu_4NPF_6 (purriss. Fluka, Merck, Darmstadt, Germany), were used as received.

3.2. Syntheses

3.2.1. *Meso*-Tetrakis(3,4,5-Trimethoxyphenyl)Porphyrin (H_2TTMPP)

Here, 3,4,5-trimethoxybenzaldehyde (363 mg, 1.85 mmol) and pyrrole (127 µL, 1.85 mmol) were added to a 250 mL of distilled $CHCl_3$ in a double-necked round bottom flask under argon and shielded from light. $BF_3{\cdot}OEt_2$ (192 µL, 0.0015 mol) was added, and the reaction was maintained at room temperature for 2 h. A few drops of NEt_3 and 179 mg. of *p*-chloranil (1.66 mmol, 0.75 equivalents) were added, and the solution was heated to reflux (light protection was removed). After 1 h, the obtained solution was cooled to room temperature. The reaction mixture was evaporated to dryness, the residue dissolved in $CHCl_3$, filtered over silica, and recrystallized from $CHCl_3$/*n*-hexane (8:2). Yield: 126 mg (0.12 mmol, 70%) of a purple solid. Anal. calcd. for $C_{56}H_{54}O_{12}N_4$ (974.37): C, 68.98; H, 5.58; N, 5.75; found: C, 68.92; H, 5.55; N, 5.71%; MS (ESI(+), CH_2Cl_2): m/z = 974.38 for $[M]^+$; UV-vis (CH_2Cl_2): λ_{max} (ε 10^{-3} $M^{-1}cm^{-1}$): 424(365), 520(78),556(41),598(24),652(32); ^{1}H NMR (500 MHz, $CDCl_3$) δ = 9.01 (s, 8H, β-pyrrole), 7.48 (s, 8H, arylH), 4.23 (s, 24H, OCH_3), 4.01 (s, 12H, OCH_3) ppm, −2.73 (s, 2H, NH) ppm. FT-IR (solid, $\bar{\bar{\nu}}$, cm^{-1}); 3328 (w), 2973 (s), 2942 (s), 2885 (m), 1745 (m), 1604 (m), 1505 (s), 1462 (m), 1288 (vs), 1235 (vs), 1164 (s), 1107 m), 1032 (s), 956 (s), 802 (vs), 734 (vs), 592 (s), 530 (s), 421 (m).

3.2.2. *Meso*-Tetrakis(3,4,5-Trimethoxyphenyl)Porphyrinato Cobalt(II) [Co(TTMPP)]

H_2TTMPP (0.200 g, 0.2 mmol) was dissolved in a mixture of $CHCl_3$ (8 mL) and EtOH (2 mL), followed by the addition of $Co(OAc)_2{\cdot}4H_2O$ (0.300 g, 1.2 mmol) and *N,N*-diisopropylethylamine (DIPEA) (0.073 mL, 0.42 mmol). The reaction mixture was stirred under an inert atmosphere of argon and under reflux at 55 °C for 1 h followed by extraction with $CHCl_3$ (15 mL) and H_2O (15 mL) six times (*interleaved*). The product was purified by silica gel column chromatography using CH_2Cl_2/ethyl acetate (7:3) as eluent. The resulting solid was filtered, washed with *n*-hexane, and finally dried under vacuum to yield 191 mg (0.18 mmol, 92.6%) of product. Anal. calcd. for $C_{56}H_{52}N_4O_{12}Co$ (1031.29): C, 65.18; H, 5.08; N, 5.43; found: C, 65.15; H, 5.06; N, 5.41%; MS (ESI(+), CH_2Cl_2): m/z = 1031.29 for $[M]^+$; UV-vis (CH_2Cl_2): λ_{max} (ε 10^{-3} $M^{-1}cm^{-1}$): 414(356), 536(47), 573 sh(18); ^{1}H NMR (500 MHz, $CDCl_3$): δ = 16.32 (s, 8H, β-pyrrole); 12.67 (s, 8H, arylH); 5.48 (s, 12H, OCH_3), 5.01 (s, 24H, OCH_3); FT-IR (solid, $\bar{\nu}$, cm^{-1}); 3063 (w), 2962 (s), 2928 (vs), 2859 (s), 1725 (vs), 1606 (m), 1456 (s), 1381 (m), 1273 (vs), 1123 (vs), 1072 (vs), 1043 (m), 957 (m), 740 (s), 699 (m), 648 (w).

3.3. Methods and Instrumentation

UV-vis absorption spectra were recorded on a WinASPECT PLUS (validation for SPECORD PLUS version 4.2) scanning spectrophotometer (Analytic, Jena, Germany) using 10 mm path length cuvettes. FT-IR spectra were measured on a Perkin Elmer Spectrum Two FT-IR spectrometer (Perkin Elmer, Darmstadt, Germany). The ^{1}H NMR spectra were measured on Bruker DPX 500 spectrometers (Bruker, Rheinhausen, Germany) in solution in deuterated solvents based on the solvent peak as an internal standard. Elemental analysis and mass spectrometry were practiced in the nanobio chemistry platform of the ICMG, Grenoble, France. A Fluoromax-4 spectrofluorometer (Horiba Scientific, Loos, France) to record photoluminescence (PL) spectra at room temperature in CH_2Cl_2. PL quantum yield (Φ_{PL}) was determined using the optical method [77] with [Zn(TPP)] as standard (Φ_{PL} = 0.031). The lifetimes were measured upon irradiation at λ = 405 nm using the single photon counting technique and the fluorescence decay was fitted to single exponentials with the PicoQuant FLUOFIT software (PicoQuant, Berlin, Germany).

3.4. Electrochemistry

Cyclic voltammetry experiments were performed using a CH-660B potentiostat (CH Instruments, Austin, TX, USA) or a Metrohm µstat400 (Metrohm, Filderstadt, Germany) at room temperature. All measurements were performed in DMF (freshly distilled) with a solute concentration of approximately 10^{-3} M and *n*-Bu_4NBF_4 (0.1 M) as supporting electrolyte. A three-electrode cell was set up with a glassy carbon working electrode, a Pt wire as counter electrode, and an Ag/$AgNO_3$ reference electrode. Potentials were converted into values for the saturated calomel electrode (SCE) by applying Equation (7) [6,9,13,78]:

$$E(\text{SCE}) = E(\text{Ag}/\text{AgNO}_3) + 360\ \text{mV} \tag{7}$$

NHE potentials are converted into the current SCE scale by subtracting about 240 mV, whereas SCE differs from the ferrocene/ferrocenium couple by +160 mV [78].

3.5. Electrocatalytic CO_2 Reduction

The experiments were performed at room temperature under a CO_2 atmosphere in a conventional three-electrode cell sealed with Apiezon M vacuum grease (Sigma Aldrich/Merck, Darmstadt, Germany). A glassy carbon electrode plate (2 cm^2, 0.25 mm thickness) was used as working electrode in the cathodic compartment. A 0.5 mm diameter platinum wire (10 cm length) was used as counter electrode in the anodic compartment. The cell was charged with the catalyst and then purged with argon or CO_2 for a minimum of 15 min before controlled potential electrolysis was carried out. Constant magnetic stirring was applied during electrolysis.

3.6. Gas Chromatography (GC)

Gas detection was performed using GC/MS gas chromatography (Perkin Elmer Clarus 560; Perkin Elmer, Darmstadt, Germany) instrument with a thermal conductivity detector fitted with RT-QPlot pre-column + molecular sieve 5 Å column. Temperature was held at 150 °C for the detector and 80 °C for the oven. The carrier gas was helium. Manual injections of 100 µL were performed during the experiment via a gas-tight Hamilton microsyringe. The total volume of the cell was 173 mL.

3.7. Faradaic Efficiency, Turnover Number, Turnover Frequency Calculation

The faradaic efficiency (FE) of CO_2 and the hydrogen evolution reaction (HER) were calculated using Equation (8):

$$\text{FE} = Z\,n\,F/Q \tag{8}$$

where Z is the amount of product in mol, n is the number of electrons (2 for both CO and H_2), F is the Faraday constant, and Q is the number of electrons (or charge) passed through the solution during electrolysis.

3.8. Gas Phase Analyses

Gas phases were analyzed by GC and the Turnover Number (TON) was calculated based on the total amount of the products in mmol in the gas phase (CO and H_2) by different porphyrin catalysts, divided by the total amount of each individual catalyst in the electrolysis solution (Equation (9)).

$$\text{TON} = n(\text{product})/n(\text{catalyst}) \tag{9}$$

The turnover frequency (TOF) was calculated using TON divided by the time of the electrolysis (Equation (10)):

$$\text{TOF} = n(\text{product})/n(\text{catalyst})/t \tag{10}$$

The n(catalyst) is calculated based on the following equation (Equation (11)):

$$n_{(\text{cat})} = \text{C}_{(Cat)} \times V_{sol} \tag{11}$$

3.9. Photo-Decomposition of RhB and MB with H_2O_2

The photocatalytic reaction was performed in a quartz tube reactor (Sigma Aldrich, Merck, Paris, France). A total of 25 mg (0.024) mmol of [Co(TTMPP)] was dispersed in aqueous solutions of MB (M_W = 319.85 g/mol) or RhB (479.03 g/mol) (both 0.05 mmol).

Before irradiation, the suspensions were stirred for 90 min in the dark in order to reach an adsorption–desorption equilibrium of the dye molecules on the surface of the catalysts. Then H_2O_2 (0.006 mmol) was added and the solutions were irradiated. During the photoreaction, about 3 mL of suspension was collected at different time intervals and centrifuged to remove solid materials. The concentrations of the dyes were determined by recording the UV-vis absorption of the supernatant at 555 nm (RhB) and 654 nm (MB). The efficiency was calculated using (Equation (12)):

$$\text{Yield (\%)} = (C_0 - C_t/C_0) * 100 \tag{12}$$

where C_0 is the initial concentration of dyes and C_t is the concentration at different time intervals.

For the catalyst recycling experiments, the solid catalyst was filtered off after each cycle and washed with water and EtOH (five times each). Then the catalyst was dried at 60 °C for 12 h and re-dispersed in fresh MB or RB solutions.

3.10. Oxidative Photodegradation Mechanism–Trapping Experiments

A small number of scavengers (5 mmol/L) were added in the dark to the aqueous RhB or MB solution before adding the solid catalysts and starting the irradiation.

4. Conclusions

The previously reported *meso*-tetrakis(3,4,5-trimethoxyphenyl)porphyrin (H_2TTMPP) and its cobalt(II) complex [Co(TTMPP)] were synthesized and for the first time characterized by IR spectroscopy, UV-vis absorption and photoluminescence spectroscopy, as well as by cyclic voltammetry (CV). CVs of [Co(TTMPP)] showed two fully reversible reduction waves at $E_{1/2} = -0.88$ V and $E_{1/2} = -2.03$ V vs. SCE assignable to Co-centered reduction. The first oxidation process at 0.3 V is reversible and assigned to the Co(II)/Co(III) couple. A second two-electron oxidation follows at 0.96 V and is very probably porphyrin-based. Using [Co(TTMPP)] as a homogeneous catalyst for the electrochemical formation of H_2 from DMF/TFA and DMF/EtN_3BF_4, we found faradaic efficiencies (FE) of 76% and 88%, respectively, upon electrolysis at −2 V. At similar potentials, the reduction in CO_2 to CO in DMF under a CO_2 atmosphere was catalyzed in the presence of TFE and PhOH as proton sources with high FEs of 95% and 88%, respectively, good turnover frequencies of 15.80 s^{-1} (TFE) and 13.85 $s^{-}1$ (PhOH), and only traces of H_2 as a by-product. Remarkably, the reaction rates of both H^+ and CO_2 reduction reactions were higher than for the parent [Co(TPP)] complex, although the applied potentials were quite similar. We found that the performance of both H^+ and CO_2 reduction is strongly dependent on the proton source and in future experiments we will study this in more detail. Additionally, the application of supported, thus heterogenized, Co(II) porphyrins seems to be an interesting venue to achieve lower potentials, higher turnover numbers and frequencies, and higher stability.

Further, the dyes methylene blue and rhodamine B were photodecomposed using H_2O_2 and [Co(TTMPP)] as solid heterogeneous catalysts with an efficiency of 84.1% and 92.6%, respectively, in 90 min under visible light irradiation. Trapping experiments of reactive oxygen species (ROS) show that holes play only a minor role in the photodegradation of RhB and MB, whereas ($^{\bullet}$OH) and ($^{\bullet}O_2{}^{-}$) are the predominant species. The [Co(TTMPP)] as a solid photocatalyst was found to be photostable over five reaction cycles. Also for the degradation, C-based supports might pave the future way to even more efficient catalysts.

Supplementary Materials: The following are available online at https://www.mdpi.com/article/10.3390/inorganics11010006/s1, Figure S1: FT-IR spectra of powder samples of H_2TTMPP and [Co(TTMPP)]. Figure S2: 500 MHz ^{1}H NMR spectrum of [Co(TTMPP)] in $CDCl_3$. Figure S3: ESI-MS(+) of [Co(TTMPP)]. Figure S4: CVs of [Co(TTMPP)] (1 mM) in the absence or in the presence of 1 to 3 eq. TFA in DMF at 250 mV s^{-1} under an Ar atmosphere and blank test without catalyst. Figure S5: GC trace of evolved H_2 gas from controlled potential electrolysis of [Co(TTMPP)] in 0.1 M *n*-Bu_4NBF_4/DMF under an Ar atmosphere with 3 eq. TFA or with 3 eq. $HNEt_3{}^+$. Figure S6: CVs of 1 mM solutions of [Co(TTMPP)] in 0.1 M *n*-Bu_4NBF_4/DMF in the absence of TFE and in the presence of 1 mM of TFE under an Ar atmosphere or under CO_2 atmosphere and blank test in the presence of 1 mM of TFE without catalyst. Figure S7: GC trace of evolved hydrogen and CO_2 gas from controlled potential electrolysis of [Co(TTMPP)] in in 0.1 M *n*-Bu_4NBF_4/DMF under a CO_2 atmosphere with: 3 eq. PhOH and with 3 eq. TFE. Figure S8: CVs of [Co(TTMPP)] in CO_2-saturated DMF with 0.1 M *n*-Bu_4NBF_4 and 1 eq TFE, scan rate varying from 250 to 1000 mV·s^{-1} and lots of $(I_{cat}/I_p)^2$ values against $1/v$. Figure S9: CVs of [Co(TTMPP)] in CO_2-saturated DMF with 0.1 M *n*-Bu_4NBF_4 and 1 eq PhOH, scan rate varying from 250 to 1000 mV·s^{-1} and plots of $(I_{cat}/I_p)^2$ values against $1/v$. Figure S10: UV-vis absorption spectra of an aliquot of the solution of [Co(TTMPP)] in DMF before and after a controlled-potential electrolysis, with 1 eq. PhOH or with 1 eq. TFE. Figure S11: A: Evolution of the absorbance of MB over time in H_2O at pH = 7 and 25 °C; 0.024 mmol [Co(TTMPP)], C_{dye} = 0.05 mmol, C_{H2O2} = 0.06 mmol and changes in $\ln(C_t/C_0)$ over time for both dyes. Figure S12: Consecutive runs in the photocatalytic of 0.05 mmol RhB or MB in the presence of 0.024 mmol [Co(TTMPP)] in H_2O at pH = 7 and in the presence 0.06 mmol of H_2O_2.

Author Contributions: Conceptualization: H.N., M.G. and A.K. (Axel Klein); methodology: H.N., F.L., M.G. and A.K. (Axel Klein); investigation: M.G., F.M., A.K. (Azhar Kechiche) and J.H.; resources: H.N. and F.L.; data curation: M.G., F.L, J.H., A.K. (Azhar Kechiche) and A.K. (Axel Klein); visualization: M.G., J.H. and A.K. (Axel Klein); supervision and project administration: H.N.; manuscript original draft: M.G.; manuscript editing: M.G. and A.K. (Axel Klein) All authors have read and agreed to the published version of the manuscript.

Funding: The authors are grateful to the Tunisian Ministry of Higher Education and Scientific Research for financial support.

Institutional Review Board Statement: Not applicable.

Informed Consent Statement: Not applicable.

Data Availability Statement: The data is available on request from the authors.

Acknowledgments: The authors also thank the University of Cologne and the University of Grenoble Alpes for their support.

Conflicts of Interest: The authors declare no conflict of interest.

References

1. Sun, T.; Zhang, Z.; Xu, J.; Liang, L.; Mai, C.-L.; Ren, L.; Zhou, Q.; Yu, Y.; Zhang, B.; Gao, P. Structural, photophysical, electrochemical and spintronic study of first-row metal Tetrakis(*meso*-triphenylamine)-porphyrin complexes: A combined experimental and theoretical study. *Dye. Pigm.* **2021**, *193*, 109469. [CrossRef]
2. Zhang, R.; Warren, J.J. Recent Developments in Metalloporphyrin Electrocatalysts for Reduction of Small Molecules: Strategies for Managing Electron and Proton Transfer Reactions. *ChemSusChem* **2021**, *14*, 293–302. [CrossRef] [PubMed]
3. Ke, X.; Kumar, R.; Sankar, M.; Kadish, K.M. Electrochemistry and Spectroelectrochemistry of Cobalt Porphyrins with π-Extending and/or Highly Electron-Withdrawing Pyrrole Substituents. *In Situ* Electrogeneration of σ-Bonded Complexes. *Inorg. Chem.* **2018**, *57*, 1490–1503. [CrossRef] [PubMed]
4. Ye, L.; Fang, Y.; Ou, Z.; Xue, S.; Kadish, K.M. Cobalt Tetrabutano- and Tetrabenzotetraarylporphyrin Complexes: Effect of Substituents on the Electrochemical Properties and Catalytic Activity of Oxygen Reduction Reactions. *Inorg. Chem.* **2017**, *56*, 13613–13626. [CrossRef] [PubMed]
5. Ke, X.; Yadav, P.; Cong, L.; Kumar, R.; Sankar, M.; Kadish, K.M. Facile and Reversible Electrogeneration of Porphyrin Trianions and Tetraanions in Nonaqueous Media. *Inorg. Chem.* **2017**, *56*, 8527–8537. [CrossRef]
6. Klein, A. Spectroelectrochemistry of Metalloporphyrins. In *Spectroelectrochemistry*; Kaim, W., Klein, A., Eds.; RSC Publishing: Cambridge, UK, 2008; pp. 91–122. ISBN 978-1-84755-840-4.
7. Sun, H.; Smirnov, V.V.; DiMagno, S.G. Slow Electron Transfer Rates for Fluorinated Cobalt Porphyrins: Electronic and Conformational Factors Modulating Metalloporphyrin ET. *Inorg. Chem.* **2003**, *42*, 6032–6040. [CrossRef]
8. Chaudhri, N.; Cong, L.; Bulbul, A.S.; Grover, N.; Osterloh, W.R.; Fang, Y.; Sankar, M.; Kadish, K.M. Structural, Photophysical, and Electrochemical Properties of Doubly Fused Porphyrins and Related Fused Chlorins. *Inorg. Chem.* **2020**, *59*, 1481–1495. [CrossRef]
9. Guergueb, M.; Loiseau, F.; Molton, F.; Nasri, H.; Klein, A. CO_2 to CO Electroreduction, electrocatalytic H_2 evolution, and catalytic degradation of organic dyes using a Co(II) *meso*-tetraarylporphyrin. *Molecules* **2022**, *27*, 1705. [CrossRef]
10. Liu, Y.; Fu, L.-Z.; Yang, L.-M.; Liu, X.-P.; Zhan, S.-Z.; Ni, C.-L. The impact of modifying the ligands on hydrogen production electro-catalyzed by *meso*-tetra-*p*-X-phenylporphin cobalt complexes, CoT(X)PP. *J. Mol. Catal. A Chem.* **2016**, *417*, 101–106. [CrossRef]

11. Nasri, S.; Hajji, M.; Guergueb, M.; Dhifaoui, S.; Marvaud, V.; Loiseau, F.; Molton, F.; Roisnel, T.; Guerfel, T.; Nasri, H. Spectroscopic, Electrochemical, Magnetic and Structural Characterization of an hexamethylenetetramine Co(II) Porphyrin Complex–Application in the Catalytic Degradation of Vat Yellow 1 dye. *J. Mol. Struct.* **2021**, *1231*, 129676. [CrossRef]
12. Guergueb, M.; Nasri, S.; Brahmi, J.; Al-Ghamdi, Y.O.; Loiseau, F.; Molton, F.; Roisnel, T.; Guerineau, V.; Nasri, H. Spectroscopic characterization, X-ray molecular structures and cyclic voltammetry study of two (piperazine) cobalt(II) *meso*-arylporphyin complexes. Application as a catalyst for the degradation of 4-nitrophenol. *Polyhedron* **2021**, *209*, 115468. [CrossRef]
13. Guergueb, M.; Nasri, S.; Brahmi, J.; Loiseau, F.; Molton, F.; Roisnel, T.; Guerineau, V.; Turowska-Tyrk, I.; Aouadi, K.; Nasri, H. Effect of the coordination of π-acceptor 4-cyanopyridine ligand on the structural and electronic properties of *meso*-tetra(*para*-methoxy) and *meso*-tetra(*para*-chlorophenyl) porphyrin cobalt(II) coordination compounds. Application in the catalytic degradation of methylene blue dye. *RSC Adv.* **2020**, *10*, 6900–6918. [CrossRef] [PubMed]
14. Pamin, K.; Tabor, E.; Gjrecka, S.; Kubiak, W.W.; Rutkowska-Zbik, D.; Połtowicz, J. Three Generations of Cobalt Porphyrins as Catalysts in the Oxidation of Cycloalkanes. *ChemSusChem* **2019**, *12*, 684–691. [CrossRef] [PubMed]
15. Hu, X.-M.; Rønne, M.H.; Pedersen, S.U.; Skrydstrup, T.; Daasbjerg, K. Enhanced Catalytic Activity of Cobalt Porphyrin in CO_2 Electroreduction upon Immobilization on Carbon Materials. *Angew. Chem. Int. Ed.* **2017**, *56*, 6468–6472. [CrossRef]
16. Lin, S.; Diercks, C.S.; Zhang, Y.-B.; Kornienko, N.; Nichols, E.M.; Zhao, Y.; Paris, A.R.; Kim, D.; Yang, P.; Yaghi, O.M.; et al. Covalent organic frameworks comprising cobalt porphyrins for catalytic CO_2 reduction in water. *Science* **2015**, *349*, 1208–1221. [CrossRef]
17. Harvey, P.D. Porphyrin-based MOFs as heterogeneous photocatalysts for the eradication of organic pollutants and toxins. *J. Porphyr. Phthalocyanines* **2021**, *25*, 583–604. [CrossRef]
18. Amiri, N.; Guergueb, M.; Al-Fakeh, M.S.; Bourguiba, M.; Nasri, H. A new cobalt(II) meso-porphyrin: Synthesis, characterization, electric properties and application in catalytic degradation of dyes. *RSC Adv.* **2020**, *10*, 44920–44932. [CrossRef]
19. Nishiori, D.; Wadsworth, B.L.; Reyes Cruz, E.A.; Nguyen, N.P.; Hensleigh, L.K.; Karcher, T.; Moore, G.F. Photoelectrochemistry of metalloporphyrin-modified GaP semiconductors. *Photosynth. Res.* **2022**, *151*, 195–204. [CrossRef]
20. Hong, Y.H.; Han, J.W.; Jung, J.; Nakagawa, T.; Lee, Y.-M.; Nam, W.; Fukuzumi, S. Photocatalytic Oxygenation Reactions with a Cobalt Porphyrin Complex Using Water as an Oxygen Source and Dioxygen as an Oxidant. *J. Am. Chem. Soc.* **2019**, *141*, 9155–9159. [CrossRef]
21. Li, W.; He, X.; Ge, R.; Zhu, M.; Feng, L.; Li, Y. Cobalt porphyrin (CoTCPP) advanced visible light response of g-C_3N_4 nanosheets. *Sust. Mater. Technol.* **2019**, *22*, e00114. [CrossRef]
22. Francis, S.; Rajith, L. Selective Fluorescent Sensing of Adenine Via the Emissive Enhancement of a Simple Cobalt Porphyrin. *J. Fluoresc.* **2021**, *31*, 577–586. [CrossRef] [PubMed]
23. Delmarre, D.; Bied-Charreton, C. Grafting of cobalt porphyrins in sol–gel matrices: Application to the detection of amines. *Sens. Actuators B Chem.* **2000**, *62*, 136–142. [CrossRef]
24. Lawrence, M.A.W.; Celestine, M.J.; Artis, E.T.; Joseph, L.S.; Esquivel, D.L.; Ledbetter, A.J.; Cropek, D.M.; Jarrett, W.L.; Bayse, C.A.; Brewer, M.I.; et al. Computational, electrochemical, and spectroscopic studies of two mononuclear cobaloximes: The influence of an axial pyridine and solvent on the redox behaviour and evidence for pyridine coordination to cobalt(I) and cobalt(II) metal centres. *Dalton Trans.* **2016**, *45*, 10326–10342. [CrossRef]
25. Kaim, W.; Schwederski, B.; Klein, A. *Bioinorganic Chemistry: Inorganic Elements in the Chemistry of Life–An Introduction and Guide*, 2nd ed.; John Wiley & Sons: Chichester, UK, 2013; ISBN 978-0-470-97523-7.
26. Simonova, O.R.; Zdanovich, S.A.; Zaitseva, S.V.; Koifman, O.I. Kinetic Study of the Redox Properties of [5,10,15,20-Tetrakis(2,5-dimethoxyphenyl)porphyrinato]cobalt(II) in the Reaction with Hydrogen Peroxide. *Russ. J. Gen. Chem.* **2020**, *90*, 863–869. [CrossRef]
27. Pu, G.; Yang, Z.; Wu, Y.; Wang, Z.; Deng, Y.; Gao, Y.J.; Zhang, Z.; Lu, X. Investigation into the Oxygen-Involved Electrochemiluminescence of Porphyrins and Its Regulation by Peripheral Substituents/Central Metals. *Anal. Chem.* **2019**, *91*, 2319–2328. [CrossRef] [PubMed]
28. Lin, X.Q.; Boisselier-Cocolios, B.; Kadish, K.M. Electrochemistry, Spectroelectrochemistry, and Ligand Addition Reactions of an Easily Reducible Cobalt Porphyrin. Reactions of Tetracyanotetraphenylporphinato)cobalt(II) ($(CN)_4TPPCo^{II}$) in Pyridine and in Pyridine/Methylene Chloride Mixtures. *Inorg. Chem.* **1986**, *25*, 3242–3248. [CrossRef]
29. Mansour, A.; Belghith, Y.; Belkhiria, M.S.; Bujacz, A.; Guérineau, V.; Nasri, H. Synthesis, crystal structures and spectroscopic characterization of Co(II) bis(4,4′-bipyridine) with mesoporphyrins α,β,α,β-tetrakis(*o*-pivalamidophenyl) porphyrin (α,β,α,β-TpivPP) and tetraphenylporphyrin (TPP). *J. Porphyr. Phthalocyanines* **2013**, *17*, 1094–1103. [CrossRef]
30. Puerres, H.; Díaz, M.; Hurtado, J.; Ortiz, P.; Cortés, M.T. Photoelectrochemical Stability under Anodic and Cathodic Conditions of Meso-Tetra-(4-Sulfonatophenyl)-Porphyrinato Cobalt (II) Immobilized in Polypyrrole Thin Films. *Polymers* **2021**, *13*, 657. [CrossRef]
31. Smith, P.T.; Benke, B.P.; An, L.; Kim, Y.; Kim, K.; Chang, C.J. A Supramolecular Porous Organic Cage Platform Promotes Electrochemical Hydrogen Evolution from Water Catalyzed by Cobalt Porphyrins. *ChemElectroChem* **2021**, *8*, 1653–1657. [CrossRef]
32. Lv, X.; Chen, Y.; Wu, Y.; Wang, H.; Wang, X.; Wei, C.; Xiao, Z.; Yang, G.; Jiang, J. A Br-regulated transition metal active-site anchoring and exposure strategy in biomass derived carbon nanosheets for obtaining robust ORR/HER electrocatalysts at all pH values. *J. Mater. Chem. A* **2019**, *7*, 27089–27098. [CrossRef]

33. Wu, Y.; Veleta, J.M.; Tang, D.; Price, A.D.; Botez, C.E.; Villagrán, D. Efficient electrocatalytic hydrogen gas evolution by a cobalt–porphyrin-based crystalline polymer. *Dalton Trans.* **2018**, *47*, 8801–8806. [CrossRef] [PubMed]
34. Yuan, Y.-J.; Yu, Z.-T.; Chen, D.-Q.; Zou, Z.-G. Metal-complex chromophores for solar hydrogen generation. *Chem. Soc. Rev.* **2017**, *46*, 603–631. [CrossRef] [PubMed]
35. Pal, R.; Laureanti, J.A.; Groy, T.L.; Jones, A.K.; Trovitch, R.J. Hydrogen production from water using a bis(imino)pyridine molybdenum electrocatalyst. *Chem. Commun.* **2016**, *52*, 11555–11558. [CrossRef] [PubMed]
36. Zee, D.Z.; Chantarojsiri, T.; Long, J.R.; Chang, C.J. Metal polypyridyl catalysts for electro- and photochemical reduction of water to hydrogen. *Acc. Chem. Res.* **2015**, *48*, 2027–2036. [CrossRef]
37. McKone, J.R.; Marinescu, S.C.; Brunschwig, B.S.; Winkler, J.J.; Gray, H.B. Earth-abundant hydrogen evolution electrocatalysts. *Chem. Sci.* **2014**, *5*, 865–878. [CrossRef]
38. Roubelakis, M.M.; Bediako, D.K.; Dogutan, D.K.; Nocera, G. Proton-coupled electron transfer kinetics for the hydrogen evolution reaction of hangman porphyrins. *Energy Environ. Sci.* **2012**, *5*, 7737–7740. [CrossRef]
39. Du, P.; Eisenberg, R. Catalysts made of earth-abundant elements (Co, Ni, Fe) for water splitting: Recent progress and future challenges. *Energy Environ. Sci.* **2012**, *5*, 6012–6021. [CrossRef]
40. Artero, V.; Chavarot-Kerlidou, M.; Fontecave, M. Splitting water with cobalt. *Angew. Chem. Int. Ed.* **2011**, *50*, 7238–7266. [CrossRef]
41. Kellett, R.M.; Spiro, T.G. Cobalt(I) porphyrin catalysts of hydrogen production from water. *Inorg. Chem.* **1985**, *24*, 2373–2377. [CrossRef]
42. Attatsi, I.K.; Weihua Zhu, W.; Liang, X. Noncovalent immobilization of Co(II)porphyrin through axial coordination as an enhanced electrocatalyst on carbon electrodes for oxygen reduction and evolution. *New J. Chem.* **2020**, *44*, 4340–4345. [CrossRef]
43. Wang, Y.-H.; Schneider, P.E.; Goldsmith, Z.K.; Mondal, B.; Hammes-Schiffer, S.; Stahl, S.S. Brønsted Acid Scaling Relationships Enable Control Over Product Selectivity from O_2 Reduction with a Mononuclear Cobalt Porphyrin Catalyst. *ACS Cent. Sci.* **2019**, *5*, 1024–1034. [CrossRef] [PubMed]
44. Wu, Z.-S.; Chen, C.; Liu, J.; Parvez, K.; Liang, H.; Shu, J.; Sachdev, H.; Graf, R.; Feng, X.; Müllen, K. High-Performance Electrocatalysts for Oxygen Reduction Derived from Cobalt Porphyrin-Based Conjugated Mesoporous Polymers. *Adv. Mater.* **2014**, *26*, 1450–1455. [CrossRef] [PubMed]
45. Mukhopadhyay, S.; Basu, O.; Das, S.K. ZIF-8 MOF Encapsulated Co-porphyrin, an Efficient Electrocatalyst for Water Oxidation in a Wide pH Range: Works Better at Neutral pH. *ChemCatChem.* **2020**, *12*, 5430–5438. [CrossRef]
46. Long, C.; Wan, K.; Qiu, X.; Zhang, X.; Han, J.; An, P.; Yang, Z.; Li, X.; Guo, J.; Shi, X.; et al. Single site catalyst with enzyme-mimic micro-environment for electroreduction of CO_2. *Nano Res.* **2022**, *15*, 1817–1823. [CrossRef]
47. Usman, M.; Humayun, M.; Garba, M.D.; Ullah, L.; Zeb, Z.; Helal, A.; Suliman, M.H.; Alfaifi, B.Y.; Iqbal, N.; Abdinejad, M.; et al. Electrochemical Reduction of CO_2: A Review of Cobalt Based Catalysts for Carbon Dioxide Conversion to Fuels. *Nanomaterials* **2021**, *11*, 2029. [CrossRef]
48. Marianov, A.N.; Kochubei, A.S.; Roman, T.; Conquest, O.J.; Stampfl, C.; Jiang, Y. Modeling and Experimental Study of the Electron Transfer Kinetics for Non-ideal Electrodes Using Variable-Frequency Square Wave Voltammetry. *Anal. Chem.* **2021**, *93*, 10175–10186. [CrossRef]
49. Dou, S.; Sun, L.; Xi, S.; Li, X.; Su, T.; Fan, H.J.; Wang, X. Enlarging the π-Conjugation of Cobalt Porphyrin for Highly Active and Selective CO_2 Electroreduction. *ChemSusChem* **2021**, *14*, 2126–2132. [CrossRef]
50. Marianov, A.N.; Kochubei, A.S.; Roman, T.; Conquest, O.J.; Stampfl, C.; Jiang, Y. Resolving Deactivation Pathways of Co Porphyrin-Based Electrocatalysts for CO_2 Reduction in Aqueous Medium. *ACS Catal.* **2021**, *11*, 3715–3729. [CrossRef]
51. Chen, X.; Hu, X.-M.; Daasbjerg, K.; Ahlquist, M.S.G. Understanding the Enhanced Catalytic CO_2 Reduction upon Adhering Cobalt Porphyrin to Carbon Nanotubes and the Inverse Loading Effect. *Organometallics* **2020**, *39*, 1634–1641. [CrossRef]
52. Jack, J.; Park, E.; Maness, P.-C.; Huang, S.; Zhang, W.; Ren, Z.J. Selective ligand modification of cobalt porphyrins for carbon dioxide electrolysis: Generation of a renewable H_2/CO feedstock for downstream catalytic hydrogenation. *Inorg. Chim. Acta* **2020**, *507*, 119594. [CrossRef]
53. Wang, Z.-j.; Song, H.; Liu, H.; Ye, J. Coupling of Solar Energy and Thermal Energy for Carbon Dioxide Reduction: Status and Prospects. *Angew. Chem. Int. Ed.* **2020**, *59*, 8016–8035. [CrossRef] [PubMed]
54. Sinha, S.; Zhang, R.; Warren, J.J. Low Overpotential CO_2 Activation by a Graphite-Adsorbed Cobalt Porphyrin. *ACS Catal.* **2020**, *10*, 12284–12291. [CrossRef]
55. Wu, Q.-J.; Mao, M.-J.; Chen, J.-X.; Huang, Y.-B.; Cao, R. Integration of metalloporphyrin into cationic covalent triazine frameworks for the synergistically enhanced chemical fixation of CO_2. *Catal. Sci. Technol.* **2020**, *10*, 8026–8033. [CrossRef]
56. Abdinejad, M.; Seifitokaldani, A.; Dao, C.; Sargent, E.H.; Zhang, X.-a.; Kraatz, H.B. Enhanced Electrochemical Reduction of CO_2 Catalyzed by Cobalt and Iron Amino Porphyrin Complexes. *ACS Appl. Energy Mater.* **2019**, *2*, 1330–1335. [CrossRef]
57. Hu, B.; Xie, W.; Li, R.; Pan, Z.; Song, S.; Wang, Y. How does the ligands structure surrounding metal-N_4 of Co-based macrocyclic compounds affect electrochemical reduction of CO_2 performance? *Electrochim. Acta* **2019**, *331*, 135283. [CrossRef]
58. Miyamoto, K.; Asahi, R. Water Facilitated Electrochemical Reduction of CO_2 on Cobalt-Porphyrin Catalysts. *J. Phys. Chem. C* **2019**, *123*, 9944–9948. [CrossRef]
59. Behar, D.; Dhanasekaran, T.; Neta, P.; Hosten, C.M.; Ejeh, D.; Hambright, P.; Fujita, E. Cobalt Porphyrin Catalyzed Reduction of CO_2, Radiation Chemical, Photochemical, and Electrochemical Studies. *J. Phys. Chem. A* **1998**, *102*, 2870–2877. [CrossRef]

60. Piccirillo, G.; Aroso, R.T.; Rodrigues, F.M.S.; Carrilho, R.M.B.; Pinto, S.M.A.; Calvete, M.J.F.; Pereira, M.M. Oxidative Degradation of Pharmaceuticals: The Role of Tetrapyrrole-Based Catalysts. *Catalysts* **2021**, *11*, 11335. [CrossRef]
61. Xie, J.; Xu, P.; Zhu, Y.; Wang, J.; Lee, W.-C.C.; Zhang, X.P. New Catalytic Radical Process Involving 1,4-Hydrogen Atom Abstraction: Asymmetric Construction of Cyclobutanones. *J. Am. Chem. Soc.* **2021**, *143*, 11670–11678. [CrossRef]
62. Li, C.; Lang, K.; Lu, H.; Hu, Y.; Cui, X.; Wojtas, L.; Zhang, X.P. Catalytic Radical Process for Enantioselective Amination of C(sp^3)–H Bonds. *Angew. Chem. Int. Ed.* **2018**, *57*, 16837–16841. [CrossRef]
63. Chan, T.L.; To, C.T.; Liao, B.-S.; Liu, S.-T.; Chan, K.S. Electronic Effects of Ligands on the Cobalt(II)–Porphyrin-Catalyzed Direct C–H Arylation of Benzene. *Eur. J. Inorg. Chem.* **2012**, *2012*, 485–489. [CrossRef]
64. Puchovskaya, S.G.; Ivanova, Y.B.; Chizhova, N.Z.; Syrbu, S.A. Synthesis, Spectral, Acid-Basic, and Coordination Properties of Bromine- and Methoxy-Substituted Tetraphenylporphyrins. *Russ. J. Gen. Chem.* **2021**, *91*, 1050–1056. [CrossRef]
65. Mishra, E.; Worlinsky, J.L.; Gilbert, T.M.; Brückner, C.; Ryzhov, V. Axial Imidazole Binding Strengths in Porphyrinoid Cobalt(III) Complexes as Studied by Tandem Mass Spectrometry. *J. Am. Soc. Mass Spectrom.* **2012**, *23*, 1135–1146. [CrossRef] [PubMed]
66. Subbaiyan, N.K.; Wijesinghe, C.A.; D'Souza, F. Supramolecular Solar Cells: Surface Modification of Nanocrystalline TiO_2 with Coordinating Ligands To Immobilize Sensitizers and Dyads via Metal-Ligand Coordination for Enhanced Photocurrent Generation. *J. Am. Chem. Soc.* **2009**, *131*, 14646–14647. [CrossRef] [PubMed]
67. Sugamoto, K.; Matsushita, Y.-i.; Matsui, T. Direct hydroperoxygenation of conjugated olefins catalyzed by cobalt(II) porphyrin. *J. Chem. Soc., Perkin Trans. 1* **1998**, *1998*, 3989–3998. [CrossRef]
68. Lindsey, J.S.; Hsu, H.C.; Schreiman, I.C. Synthesis of tetraphenylporphyrins under very mild conditions. *Tetrahedron Lett.* **1986**, *27*, 4969–4970. [CrossRef]
69. Soury, R.; Jabli, M.; Saleh, T.A.; Abdul-Hassan, W.S.; Saint-Aman, E.; Loiseau, F.; Philouze, C.; Nasri, H. Tetrakis(ethyl-4(4-butyryl)oxyphenyl)porphyrinato zinc complexes with 4,4′-bpyridine: Synthesis, characterization, and its catalytic degradation of Calmagite. *RSC Adv.* **2018**, *8*, 20143–20156. [CrossRef]
70. Chen, P.; Finikova, O.S.; Ou, Z.; Vinogradov, S.A.; Kadish, K.M. Electrochemistry of Platinum(II) Porphyrins: Effect of Substituents and π-Extension on Redox Potentials and Site of Electron Transfer. *Inorg. Chem.* **2012**, *51*, 6200–6210. [CrossRef] [PubMed]
71. Queyriaux, N.; Sun, D.; Fize, J.; Pecaut, J.; Field, M.J.; Chavarot-Kerlidou, M.; Artero, V. Electrocatalytic Hydrogen Evolution with a Cobalt Complex Bearing Pendant Proton Relays: Acid Strength and Applied Potential Govern Mechanism and Stability. *J. Am. Chem. Soc.* **2020**, *142*, 274–282. [CrossRef]
72. Gu, S.; Marianov, A.N.; Jiang, Y. Covalent grafting of cobalt aminoporphyrin-based electrocatalyst onto carbon nanotubes for excellent activity in CO_2 reduction. *Appl. Catal. B Environm.* **2022**, *300*, 120750. [CrossRef]
73. Rountree, E.S.; McCarthy, B.D.; Eisenhart, T.T.; Dempsey, J.L. Evaluation of Homogeneous Electrocatalysts by Cyclic Voltammetry. *Inorg. Chem.* **2014**, *53*, 9983–10002. [CrossRef] [PubMed]
74. Costentin, C.; Drouet, S.; Robert, M.; Saveant, J.-M. Turnover numbers, turnover frequencies, and overpotential in molecular catalysis of electrochemical reactions. Cyclic voltammetry and preparative-scale electrolysis. *J. Am. Chem. Soc.* **2012**, *134*, 11235–11242. [CrossRef] [PubMed]
75. Warren, J.J.; Tronic, T.A.; Mayer, J.M. Thermochemistry of Proton-Coupled Electron Transfer Reagents and Its Implications. *Chem. Rev.* **2010**, *110*, 6961–7001. [CrossRef] [PubMed]
76. Ait Ahsaine, H.; El Jaouhari, A.; Slassi, A.; Ezahri, M.; Benlhachemi, A.; Bakiz, B.; Guinneton, F.; Gavarri, J.-R. Electronic band structure and visible-light photocatalytic activity of Bi_2WO_6: Elucidating the effect of lutetium doping. *RSC Adv.* **2016**, *6*, 101105–101114. [CrossRef]
77. Guergueb, M.; Brahmi, J.; Nasri, S.; Loiseau, F.; Aouadi, K.; Guerineau, V.; Najmudin, S.; Nasri, H. Zinc(II) triazole meso-arylsubstituted porphyrins for UV-visible chloride and bromide detection. Adsorption and catalytic degradation of malachite green dye. *RSC Adv.* **2020**, *10*, 22712–22725. [CrossRef]
78. Connelly, N.G.; Geiger, W.E. Chemical Redox Agents for Organometallic Chemistry. *Chem. Rev.* **1996**, *96*, 877–910. [CrossRef]